On the Effects of High Order Scattering in 3D Cubical and Rectangular Furnaces

Manosh C. Paul *
Department of Mechanical Engineering, University of Glasgow,
Glasgow G12 8QQ, UK

Abstract

The discrete ordinates method (DOM/S_n) is implemented to investigate the high order scattering effects of absorbing-emitting-scattering grey gas media inside the three-dimensional cubical and rectangular furnaces. To validate the numerical method, the furnaces are considered first to be filled with non-scattering grey gases, and the results of the higher order approximations of the DOM show an excellent agreement compared with those available in the literature. The DOM is then extended to apply in the scattering media inside the furnaces, and the results of various scattering approaches such as out-scattering, iso-scattering, linear aniso-scattering and nonlinear aniso-scattering are obtained and presented in this paper.

Keywords: Discrete ordinates method, Radiative heat transfer, Scattering effects
Short title: *Scattering effects in 3D furnaces*

Nomenclature

Roman Characters

a	coefficient of the scattering phase function
A, B, C	surface areas of a control volume
I	radiative intensity
M	total number of the discrete directions
P	Legendre polynomial
q	radiative heat fluxes
sb	Stefan-Boltzmann constant
S	radiation source term
T	temperature
x_j	cartesian coordinates, (x, y, z)
V	volume

Greek Symbols

*E-mail:m.paul@mech.gla.ac.uk, Tel:+44 (0)141 330 8466, Fax:+44 (0)141 330 4343

α, β, γ	direction cosines
ϵ	emissivity
κ	absorption coefficient
ω	quadrature weight
Ω	angular direction
Φ	scattering phase function
σ	scattering coefficient

Subscripts

b	black body
in	incident
l	order of a
m	angular discrete direction
n	approximation of S_n
w	wall

Superscripts

$\bar{.}$	non-dimensional term
e, w	east and west surfaces of a control volume
n, s	north and south
l, r	left and right
P	nodal intensity
$\prime$	incoming radiative directions

Abbreviations

DOM	Discrete Ordinate Method
$IFRF$	International Flame Research Foundation
RTE	Radiative Transfer Equation

1 Introduction

In most high temperature engineering combustion devices such as boilers, furnaces, engine combustors etc, radiation becomes the dominant mode of heat transfer. The prediction of wall temperatures is an important aspect in the design of high temperature combustion devices, and this clearly requires that the radiative heat fluxes be predicted accurately. An inability to predict the wall temperatures may lead to an excessive amount of the combustor airflow being used for cooling the combustor wall and this is likely to lead to a reduced combustion efficiency and an increased emission of the pollutants such as carbon monoxide (CO), NO_x formations and unburned hydrocarbons (UHC).

To meet the world environmental regulations and for safer environment, one of the main objectives in designing of the practical combustion devices is to reduce the

pollutant emissions. The numerical study becomes a vital tool to predict the radiative heat transfer inside high temperature combustion devices, and now-a-days it is also used to replace very costly and time-consuming experimental test procedures of any devices. For example see [1, 2], where some recent work on the radiative heat transfer in a gas turbine combustion chamber are carried out.

The radiative transfer usually interacts with absorbing, emitting and scattering in a radiatively participating medium, and to obtain the net heat transfer distribution inside the medium, the radiative transfer equation (RTE) is coupled with both out-scattering and in-scattering [3].

Chandrasekhar [4] first proposed a method which is known as the Discrete Ordinates Method (DOM) in his work on one-dimensional stellar and atmospheric radiation. Subsequently Carlson and Lathrop [5] developed the DOM for multidimensional radiation problems employing the finite volume approaches. Recently, the DOM has been widely used on various different problems [see 1, 2, 6-11].

The radiative transfer equation is an integro-differential equation (Eq. (1)) with the coupling of incoming and outgoing radiative intensities. To date, most of the radiation applications are found to be in non-scattering, absorbing, emitting and grey media. If the scattering is considered, in order to calculate a single directional radiative intensity from a computational node one requires the calculation of all scattered intensities into that node, i.e. the in-scattering [3, 6, 9], and this becomes computationally a very expensive calculation. In most practical situations, a simultaneous solution of the radiative transfer equation and the fluid conservative equations such as the Navier-Stokes, enthalpy, combustion species concentrations etc are also required [2, 12], and the numerical simulation deserves a large amount of computer resources.

Among the other different numerical methods such as the Discrete Transfer Method, the Finite Volume Method and the Finite Element Method etc found in the literature, the Discrete Ordinates Method becomes a popular numerical method for radiations although it suffers by the ray effect in an optically thin media [13]. The Discrete Ordinates Method has some obvious advantages such as the simplicity of concepts, the control volume approaches etc.

In the present work, the DOM has been applied in two three-dimensional furnaces; one of them is a cubical furnace with the dimension of $1m \times 1m \times 1m$ and other is the M3 trial case (Flame 10) of the International Flame Research Foundation (IFRF) furnace with the dimension of $6m \times 2m \times 2m$ [14]. Initially, the media inside the furnaces are filled with non-scattering and absorbing-emitting grey gases and the numerical results are validated with the exact solution of [15] for the cubical furnace and with the zone method of [14] for the IFRF furnace. The furnaces are then filled with scattering and absorbing-emitting grey gases and the high order effects of the scattering are investigated. To the best of author's knowledge, the effects of scattering in these two furnaces have not been studied before, and the present paper focuses on the important issues of the radiation scattering.

2 General equation of the radiative transfer

Consider a three-dimensional cubical/rectangular furnace with the presence of an absorbing, emitting, scattering and grey medium (radiatively participating medium) inside as shown in Fig. 1. The balance of a radiative energy, which also refers to the radiative intensity, travelling in a direction of $\hat{s}$ within a small pencil of rays inside the furnace can be written as [3]

$$\Omega.\nabla I(r,\Omega) = -(\kappa+\sigma)I(r,\Omega) + \kappa I_b(r) + \frac{\sigma}{4\pi}\int_{\Omega'=4\pi} I(r,\Omega')\Phi(\Omega'\rightarrow\Omega)d\Omega' \,, \quad (1)$$

where $I(r,\Omega)$ is the radiative intensity depends on both the location vector, $r = (x,y,z)$ and the directions, Ω and Ω'; κ and σ are the absorption and the scattering coefficients respectively; $\Phi(\Omega'\rightarrow\Omega)$ is the scattering phase function which determines a probability of the radiative energy transfer from the incoming (Ω') to the outgoing (Ω) directions (see Fig. 1); $I_b(r)$ is the blackbody intensity at the temperature of the medium defined as $\frac{s_b T^4}{\pi}$, where $s_b = 5.67\times10^{-8}W/m^2K^4$ is the Stefan-Boltzmann constant and T is the temperature of the medium.

In Eq. (1), the expression of the left hand side represents the gradient of the radiative intensity in the specified direction, Ω; and the three terms on the right hand side represent changes of the radiative intensity due to the absorption and out-scattering, emission, and in-scattering respectively. In particular, the first term on the right side represents the total attenuation of the radiative intensity by both absorption and scattering, while the second and last terms are for the total augmentation of the radiative intensity by emission and scattering respectively.

2.1 Boundary conditions

The radiative transfer equation (1) is a first order quasi-steady differential equation for the intensity at a fixed direction. Consider the surfaces bounding the medium are diffusely emitting and reflective, the appropriate boundary condition for the radiative intensity leaving the wall is given as [3]

$$I(r,\Omega) = \epsilon_w I_{bw} + \frac{1-\epsilon_w}{\pi}\int_{n.\Omega'<0} I(r,\Omega')|n.\Omega'|d\Omega' \,, \quad (2)$$

where the first term on the right hand side is due to the diffusive radiative emission from the surface, while the second term is the incoming radiative heat fluxes related to the incoming radiative intensities on the surface and also known as an irradiation by which the radiative intensities reflect diffusely from the surface. I_{bw} is the black body intensity of the wall, ϵ_w is the emissivity of the wall and n is the outward unit normal vector at the boundary.

3 Discrete Ordinates Method

The discrete ordinates or S_n (where n represents the order of approximation based on a discrete representation of the directional variation of the radiative intensity) method was first proposed by Chandrasekhar [4] for the one-dimensional radiative

transfer in stellar and atmospheric physics. For a multidimensional case, the general equation of the radiative transfer (1) is usually solved for a number of different ordinate directions, and the integrals over direction on the right hand sides of Eqs. (1)-(2) are replaced by the quadrature summations [3, 5]. In a three-dimensional Cartesian coordinate system, the RTE of Eq. (1) can be rewritten as discrete ordinates form as

$$\alpha_m \frac{\partial I_m}{\partial x} + \beta_m \frac{\partial I_m}{\partial y} + \gamma_m \frac{\partial I_m}{\partial z} = -(\kappa + \sigma) I_m + \kappa I_b + \frac{\sigma}{4\pi} \sum_{m'=1}^{M} \omega_{m'} I_{m'} \Phi_{mm'} \ , \qquad (3)$$

$$m = 1, 2, ..., M$$

where the subscripts m and m' denote the outgoing and incoming radiative directions respectively; M, the total number of the discrete ordinates to be transmitted from each computational control volume is defined as $M = n(n+2)$; the terms α_m, β_m and γ_m are the direction cosines of the discrete direction $\hat{s}_m$ along the Cartesian coordinates (see Fig. 1); and $\omega_{m'}$ are the quadrature weights corresponding to the direction $\hat{s}_{m'}$. The values of the direction cosines and the corresponding quadrature weights used here can be found in [3, 6].

The scattering phase function in Eq. (3) can be expressed as a series in Legendre polynomials [16],

$$\Phi_{mm'} = \sum_{l=0}^{L} (2l+1) a_l P_l(\cos\Theta) \ , \qquad (4)$$

where $P_l(\cos\Theta)$ is the Legendre polynomials and $\cos\Theta$ can be defined as

$$\cos\Theta = \alpha_m \alpha_{m'} + \beta_m \beta_{m'} + \gamma_m \gamma_{m'} \ . \qquad (5)$$

The approximation of the scattering phase function for the iso-scattering ($L = 0$) is

$$\Phi_{mm'} = a_0 \ ; \qquad (6)$$

while for the linear aniso-scattering ($L = 1$) is

$$\Phi_{mm'} = a_0 + 3a_1(\alpha_m \alpha_{m'} + \beta_m \beta_{m'} + \gamma_m \gamma_{m'}) \ ; \qquad (7)$$

and for the nonlinear aniso-scattering ($L = 2$) is

$$\Phi_{mm'} = a_0 + 3a_1(\alpha_m \alpha_{m'} + \beta_m \beta_{m'} + \gamma_m \gamma_{m'}) + \tfrac{5}{2} a_2 \left[3(\alpha_m \alpha_{m'} + \beta_m \beta_{m'} + \gamma_m \gamma_{m'})^2 - 1 \right] \ . \qquad (8)$$

The unknown values of the scattering coefficients, a_l, in Eq. (4) may be obtained using the Mie theory. But this theory remains a very complexity in expression due to its nature. In the Mie theory, the relationships which lead to determine the scattering coefficients are involved with the frequent calculation of complicated functions with very complex arguments, and it is not a very simple task even using today's powerful computers. Therefore, a few approximations such as the Delta-Eddington [17] are used to approximate the scattering phase function in order to minimise the complexity appears in the Mie theory. But the Delta-Eddington approximation

again remains the values of the scattering coefficients as unknown and several authors used this approximation in scattering problems (e.g. see Fiveland [6]) giving the parametric values of the scattering coefficients. In this study, no approximation to the scattering coefficients is made, but we have used some parametric values for the scattering coefficients appeared in Eqs. (6)-(8).

The boundary condition given in Eq. (2) can now easily be rewritten in the discrete ordinates form (see [3]) in order to solve Eq. (3).

4 Solution algorithm

The finite volume approach of Carlson and Lathrop [5] is employed in the DOM by which a discretised form of the equation (3) can be obtained as

$$I_m^P = \frac{|\alpha_m| A I_m^w + |\beta_m| B I_m^s + |\gamma_m| C I_m^l + dS\Delta V}{|\alpha_m| A + |\beta_m| B + |\gamma_m| C + d(\kappa+\sigma)\Delta V} \tag{9}$$

with the weighted diamond differencing scheme [5, 3] shown as

$$I_m^P = dI_m^e + (1-d)I_m^w = dI_m^n + (1-d)I_m^s = dI_m^r + (1-d)I_m^l \,, \tag{10}$$

where $0.5 \leq d \leq 1$ and A, B and C represent the surface areas of the computational control volume in three directions, respectively. I_m^P, I_m^e, I_m^n and I_m^r are the nodal and surface intensities. The source term, S, for the radiation contains the contribution of the black body intensity with the absorption coefficient and the scattering term as

$$S = \kappa I_b^P + \frac{\sigma}{4\pi} \sum_{m'=1}^{M} \omega_{m'} I_{m'}^P \Phi_{mm'} \,. \tag{11}$$

It is clear that without the presence of scattering, the RTE in Eq. (9) is uncoupled with the incoming radiative intensities and may be solved independently. However, for the scattering medium, the solution of the RTE proceeds with a global iterative process described below.

At each iteration the black body intensity, the scattering phase function and the incoming scattered radiative intensities from all possible directions of $\hat{s}'_m$ at each computational node point are computed first in order to obtain the source term S given in Eq. (11). The discrete Eq. (9) is then solved in every direction of $\hat{s}_m$ and the total boundary conditions in Eq. (2) are updated for the next iteration. The new solutions are then replaced by the previous iterative solutions and this process continues until the following convergent condition is satisfied

$$\underset{1\leq m\leq M}{max} \left| I_m^{P(i+1)} - I_m^{P(i)} \right| \leq 10^{-6} \,, \tag{12}$$

where i in the number of iteration.

5 Performances of the DOM

Performances of the discrete ordinates method in both non-scattering and scattering media are separately presented here. Two problems, (i) the cubical furnace and (ii)

the International Flame Research Foundation (IFRF) furnace are considered here. Initially in Section 5.1, the DOM is applied in the non-scattering media. To examine the accuracy and the computational efficiency of the numerical method, the present numerical results are compared with those of the existing results in the literature. Finally, the devised numerical method is applied into the scattering media inside the furnaces and the results are presented in Section 5.2.

The diamond difference or symmetric scheme of the discrete ordinates method for which the corresponding value of d (see Eq. (10)) chosen to be 0.5 is found to be unstable - which is the second order accurate central difference approach. The scheme gives positive-negative oscillatory values of the radiative intensities which are physically unrealistic [18]. Fiveland [6] suggested that if the dimensions of the control volumes were kept within a range such as $dx < \frac{|\alpha|_{min}}{\kappa(1-d)}$, $dy < \frac{|\beta|_{min}}{\kappa(1-d)}$, etc, the negative intensities might be minimised but not totally avoided. Therefore, it becomes important to employ a negative intensity 'fixup' procedure such that when a negative intensity arises, the value of d will be switched to 1.0 from 0.5, or gradually increase the value of d from 0.5 to 1.0 until a stable positive solution is achieved. In our computation, the negative fixup procedure of the DOM is applied in both problems and no unphysical negative intensities are calculated. The radiation results presented here are always free from oscillation except from the fact that the scheme is turned to the first order accurate during its fixing operation. However, the results show that the scheme has a very good agreement with the exact solutions shown in non-scattering media.

5.1 Non-scattering results with the validation of DOM

We consider that the cubical and rectangular furnaces are filled with absorbing, emitting, non-scattering (for which $\sigma = 0$) and grey gases with a uniform distribution of the absorption coefficient, κ. The results of the application of the DOM in both cases are individually presented below.

5.1.1 Cubical furnace

Fig. 1 shows the geometry of the cubical furnace which contains a hot gas with the maximum temperature of T^* (reference temperature). The dimensions of this furnace are $1m$, $1m$ and $1m$ along x, y and z directions respectively, and the numerical grid employed in the simulation consists of a total of 64000 control volumes with $40 \times 40 \times 40$ grid nodes along the three coordinate directions respectively.

The furnace has six cold black walls, i.e. the temperature of those walls is of $T_w = 0$, and the absorption coefficient of the gas inside the furnace is given by $\kappa = 0.1m^{-1}$. The variation of the gas temperature inside the furnace is written as the following mathematical form as

$$2T(x, y, z) = T^* \left[1 + f(2x - 1)f(r)\right] , \tag{13}$$

where function, f, is defined as

$$f(p) = 1 - p^2 ,$$

where p is an unknown variable for f. In Eq. (13) variable r gives the temperature variation along the yz plane which is defined as

$$r = \frac{\left[(2y-1)^2 + (2z-1)^2\right]^{1/2}}{\sqrt{2}} \, .$$

This is the same mathematical form of the temperature distribution, which was used by Kim and Huh [15] for the exact solutions of the radiative heat transfer in a cubical furnace.

The temperature distribution given in Eq. (13) has a peak temperature at the centre of the furnace, and throughout the media it is distributed parabolically along the each co-ordinate direction. This approximation gives temperature at every computational grid node within the furnace and also permits to carry out the numerical experiment. Selçuk [19] also used a polynomial approximation to the gas temperature in order to study the radiative heat transfer inside a rectangular furnace.

Alternatively, when the temperature inside a media is unknown, one could assign the radiative equilibrium approach in which the radiation takes the dominant mode of heat transfer and the convection and conduction are assumed to be negligible. This approach is a good assumption for extremely high temperature applications such as nuclear explosions, plasmas etc. When the radiative equilibrium prevailed, the radiative transfer equation (3) is iteratively solved with the steady state energy balance equation, where the divergence of the radiative heat flux is related to the medium temperature and the incident radiation [3]. Some applications of the radiative equilibrium approach can be found in Menguc and Viskanta [20] and Fiveland [6].

The non-dimensional radiative heat fluxes, $\bar{q}_n = q_n/\sigma(T^*)^4$, along the centreline (at $y = 0.5m$) on the $z = L_z$ wall of the cubical furnace are plotted in Fig. 2; where the net radiative fluxes, q_n, are calculated using $q_n = \epsilon_w \left(q_{in} - \pi I_{bw}\right)$. The surrounding walls of the cubical furnace are black and kept at zero level temperature, hence the amount of the outgoing radiative heat fluxes from the surfaces, i.e. the black body intensity (I_{bw}) on the surfaces, will be zero.

The incident radiative heat fluxes, q_{in}, on the $z = L_z$ wall are calculated as

$$q_{in} = \sum_{\gamma_{m'}>0} \omega_{m'} I_{m'} |\gamma_{m'}| \, . \tag{14}$$

Fig. 2 shows that the high order approximations of the DOM such as S_6 and S_8 give an excellent agreement with the exact solutions of Kim and Huh [15], while the lower order (e.g. S_2 and S_4) results are less accurate especially where the peak heat fluxes are predicted. This can be understood by the fact that the lower order approximations of the DOM suffer by the ray effect when the medium is optically thin [13].

Kim and Huh [15] already showed that the ray effects can be reduced for an optically thick medium for which the gas absorption coefficient is considered to be greater than $\kappa = 0.1$. In the optically thick medium their predictions of DOM show better agreement with the exact solutions. In the present paper, the performances of the DOM considering various values of the absorption coefficient, κ, which are

appropriate for an optically thick medium, will not be given. Since our main intention of this section is to validate the present DOM results, and latter the chief task is to carry out investigation in the scattering media.

5.1.2 IFRF furnace

The International Flame Research Foundation (IFRF) furnace has a similar rectangular geometry as shown in Fig. 1 with the dimensions of $6m$, $2m$ and $2m$ along x, y and z respectively, which is one of the M3 trial cases (Flame 10) of the IFRF. The measured gas temperature in kelvins (K) inside the IFRF furnace are taken from the work done by Hyde and Truelove [14]. Temperature at the floor ($z = 0m$) of the furnace is kept at $320K$ while it is $1090K$ at the roof ($z = 2m$) and the side walls. The gas absorption coefficient and the emmissivity of the walls of the furnace are taken as $\kappa = 0.2m^{-1}$, $\epsilon_w = 0.86$ (on $z = 0$) and $\epsilon_w = 0.70$ (on other walls). In this case, the furnace is discretised into $45 \times 15 \times 15$ control volumes. Several researchers have studied this problem (non scattering) to validate their numerical results, for example, see Jamaluddin and Smith [7].

Fig. 3 shows the incident radiative heat fluxes, q_{in}, on the floor (Fig. 3a) and on the roof (Fig. 3b) of the IFRF furnace. These heat fluxes have been calculated using the same mathematical relation given in Eq. (14). Fig. 3a shows that the predictions of q_{in} by the higher order approximations of the DOM (e.g. S_4, S_6 and S_8) have excellent agreement compared with those of Hyde and Truelove [14] who used the zone method, while the lower order (S_2) approximation gives less accurate results. Fig. 3b also shows that on the roof ($z = 2m$) only S_6 and S_8 approximations have excellent agreement with the zone results, while the S_4 results are better than S_2.

5.2 Scattering results

In this section, we now consider that both the cubical and rectangular furnaces are filled with absorbing, emitting, scattering ($\sigma \neq 0$) and grey gases (radiatively participating media) with a uniform distribution of the absorption coefficient, κ. The scattering results are presented separately in Sections 5.2.1 and 5.2.2.

In the simulation, both the out-scattering and the in-scattering at each computational node point are considered. The media attenuate by the out-scattering, because a part of the incoming radiative intensities is removed from the direction of its propagation; see the first term of the right hand side of the equation (1) where the rate of attenuation, $-\sigma I$, is added. But for the in-scattering, the out scattered radiative intensities are redirected and appeared as augmentation of the internal energy along another direction. The rate of the scattering augmentation is added in the last term of the right hand side of the RTE (1).

Although in the previous section (for non-scattering media) we were able to assess our numerical results with those of others work, it was not possible to validate the present numerical results of the scattering effects due to an unavailability of any experimental or theoretical data/results in the open literature. However, the numerical accuracy and efficiency in the scattering media are checked carefully with

a reasonable good tolerance range of [3]

$$\frac{1}{4\pi}\int_{4\pi}\Phi(\Omega',\Omega)d\Omega' = 1\,. \tag{15}$$

In the non-scattering media the higher order approximations of the DOM/S_n are found to be more accurate in both furnaces (see Figs. 2 and 3), therefore, here in the scattering media we will apply only the S_8 approximation of the DOM and the numerical results are presented in Figs. 4-6. The negative fixup procedure is also applied here.

5.2.1 Cubical furnace

The geometry and specifications of the cubical furnace considered here are as same as given in Fig. 1, and these have already been discussed in Section 5.1.1.

The results of the non-dimensional total radiative intensities, $\bar{I} = I/\sigma(T^*)^4$, of various scattering approaches at $y = 0.5m$ and $z = 0.5m$ along the x direction are plotted in Fig. 4, where the total radiative intensities are calculated as

$$I = \sum_{m=1}^{M} I_m^P\,. \tag{16}$$

It is seen from this figure that the scattering effects has a great influence on the radiative energy storages inside the medium. The results of the radiative intensities also show their dependency on the approximation of the scattering phase function. For example, considering only the out scattering, the prediction of the total radiative intensities is lower than the non-scattering results. This is due to the fact that the radiation beams scattered out from the computational nodes by the out-scattering. Once the iso-scattering is included, for which the coefficient of the Lagendre polynomial is chosen to be $a_0 = 1.0$ (see Eq. (6)), the out scattered radiation beams now appear as in-scattering and augment the total radiative intensities and that is why that the iso-scattering result is higher than the non-scattering one.

Considering the higher order scattering approximations, such as the linear aniso-scattering for which we considered $(a_0, a_1) = (1.0, 0.8)$ and the nonlinear aniso-scattering for which we considered $(a_0, a_1, a_2) = (1.0, 0.8, 0.8)$, there appear to have some variations of the total radiative intensities near the region where the peak values of the intensities are predicted. Nonlinear effect also increases the total radiative intensities, while surprisingly the linear aniso-scattering decreases the total radiative intensities and stay slightly below the non-scattering result. However, it is interesting to note that there exists a radiatively equilibrium state near at $x = 0.1$ and $x = 0.9$ in which the linear and nonlinear scattering-absorption results are same as the absorption results (non-scattering).

Figure 5 shows the S_8 predictions of the non-dimensional net radiative heat fluxes, $\bar{q}_n$, at $y = 0.5m$ on the $z = L_z$ wall of the cubical furnace. From this figure it is clear that the scattering also has a significant influence on the prediction of the wall radiative heat fluxes. Applying various scattering approaches, the predictions of $\bar{q}_n$ are found to be lower than the non-scattering results.

5.2.2 IFRF furnace

In this section we present the scattering results in the IFRF furnace and its detailed configuration has already been described in Section 5.1.2. Figure 6a shows that for all scattering approximations such as the iso-scattering, linear aniso-scattering and nonlinear aniso-scattering, the predictions of the incident radiative heat fluxes, q_{in}, on the floor ($z = 0$) are lower than the non-scattering results. That is the wall gains less heat by the scattering mechanism. On the other hand, Figure 6b shows that by the scattering the incident radiative heat fluxes, q_{in}, on the roof ($z = 2m$) are higher than the non-scattering results, that is the roof gains more heat due to the scattering effects. In this case, the coefficients of the Lagendre polynomials in the scattering phase functions are considered as $a_0 = 1.0$, $a_1 = 0.5$ and $a_2 = 0.5$, and the value for the scattering coefficient is taken to be $\sigma = 0.5$.

6 Conclusion

The discrete ordinates method (DOM) has been applied in both scattering and non-scattering media inside the three-dimensional cubical and rectangular furnaces. To validate the numerical method, initially the DOM has been applied in the non-scattering, absorbing and emitting grey gas media, and the numerical results have been compared with the existing results available in the literature. The DOM has been extended for the higher order scattering, where the scattering phase function was expressed as a series in Legendre polynomials, and finally it has been applied into the scattering, absorbing and emitting grey gas media inside the furnaces. Both the out-scattering and the in-scattering have been considered.

The present numerical results show that the predictions of the radiative intensities and the radiative heat fluxes are highly dependent on the scattering and they are also dependent on the order of the approximations of the scattering phase function.

In many engineering applications and combustion devices, for example, burning of fuel in a combustion device, when the fact of heat transfer concerns with the formation of solid soots, the interaction of thermal radiation with an absorbing-emitting and scattering medium must be accounted for. Considering only the non-scattering approach may mislead the radiative transfer calculations, and therefore it may mislead the total heat transfer predictions.

References

[1] N. Kayakol, N. Selçuk, I. Campbell, O. L. Gulder, Performance of discrete ordinates method in a gas turbine combustor simulator, Exper. Thermal and Fluid Science 21 (2000) 134-141.

[2] W. P. Jones, M. C. Paul, Combination of DOM with LES in a Gas Turbine Combustor, Int. J. Eng. Science, 43. 379-397 2005

[3] M. F. Modest, Radiative heat transfer, Academic Press, 2003.

[4] S. Chandrasekhar, Radiative Transfer, Dover Publications, 1960.

[5] B. G. Carlson, K. D. Lathrop, Transport Theory-The Method of Discrete Ordinates, in Computing Methods in Reactor Physics, eds. H. Greespan, C. N. Kelber, and D. Okrent, Gordon and Breach, New York, 1968.

[6] W. A. Fiveland, Three-Dimensional Radiative Heat-Transfer Solutions by the Discrete-Ordinates Method, J. Thermophys 2(4) (1988) 309-316.

[7] A. S. Jamaluddin, P. J. Smith, Predicting Radiative Transfer in Rectangular Enclosures Using the Discrete Ordinates Method, Combustion Sci. Technology 59 (1988) 321-340.

[8] J. C. Chai, S. V. Patankar, H. S. Lee, Evaluation of Spatial Differencing Practices for the Discrete-Ordinates Method, J. Thermophys. and Heat Transfer 8(1) (1994) 140-144.

[9] L. H. Liu, L. M. Ruan, H. P. Tan, On the discrete ordinates method for radiative heat transfer in anisotropically scattering media, Int. J. Heat and Mass Trasnfer 45 (2002) 3259-3262.

[10] H. Koo, R. Vaillon, V. Goutiere, V. L. Dez, H. Cha, T. Song, Comparison of three discrete ordinates methods applied to two-dimensional curved geometries, Int. J. Thermal Sciences 42 (2003) 343-359.

[11] Z. Guo, K. Kim, Ultrafast-laser-radiation transfer in heterogeneous tissue with the discrete-ordinates method, Appl. Optics 42(16) (2003) 2897-2905.

[12] L. H. Howell, R. B. Pember, P Colella, J. P. Jessee, W. A. Fiveland, A conservative adaptive-mesh algorithm for unsteady, combined-mode heat transfer using the discrete ordinates method, Numer. Heat Transfer, Part B 35 (1999) 407-430.

[13] J. C. Chai, H. S. Lee, S. V. Patankar, Ray effect and False Scattering in the Discrete Ordinates Method, Numer. Heat Transfer, Part B 24 (1993) 373-389.

[14] D. J. Hyde, J. S. Truelove, The Discrete Ordinates Approximation for Multidimensional Radiant Heat Transfer in Furnaces, AERE R-8502, AERE Harwell, UK, 1977.

[15] S. H. Kim, K. Y. Huh, Assesment of the finite-volume method and the discrete ordinate method for radiative heat transfer in a three-dimensional rectangular enclosure, Numer. Heat Transfer, Part B 35 (1999) 85-112.

[16] C. M. Chu, S. W. Churchill, Representation of the angular distribution of radiation scattered by a spherical particle, J. Opt. Soc. America 45(11) (1955) 958-962.

[17] J. H. Joseph, W. J. Wiscombe, J. A. Weinman, The Delta-Eddington Approximation for Radiative Flux Transfer, J. Atmos. Science 33 (1976) 2452-2459.

[18] K. D. Lathrop, Spatial differencing the transport equation: positivity vs. accuracy, J. Comp. Physics 4 (1969) 475-498.

[19] N. Selçuk, Exact solutions for Radiative Heat Transfer in Box-Shaped Furnaces, J. Heat Transfer 107 (1985) 648-655.

[20] M. Menguc, R. Viskanta, Radiative Transfer in Three-Dimensional Rectangular Enclosures, J. Quan. Spec. Rad. Transfer 33 (1985) 533-549.

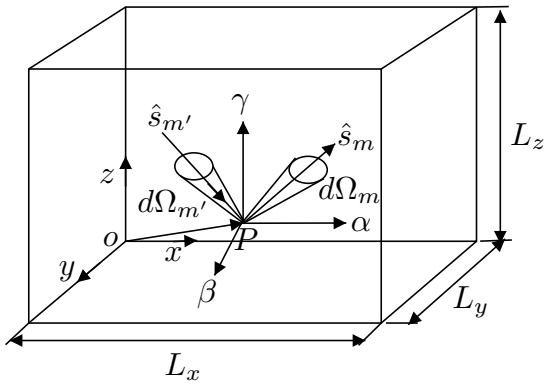

Figure 1: An orientation of the angular coordinate systems and directions for the radiative transfer in a 3D furnace.

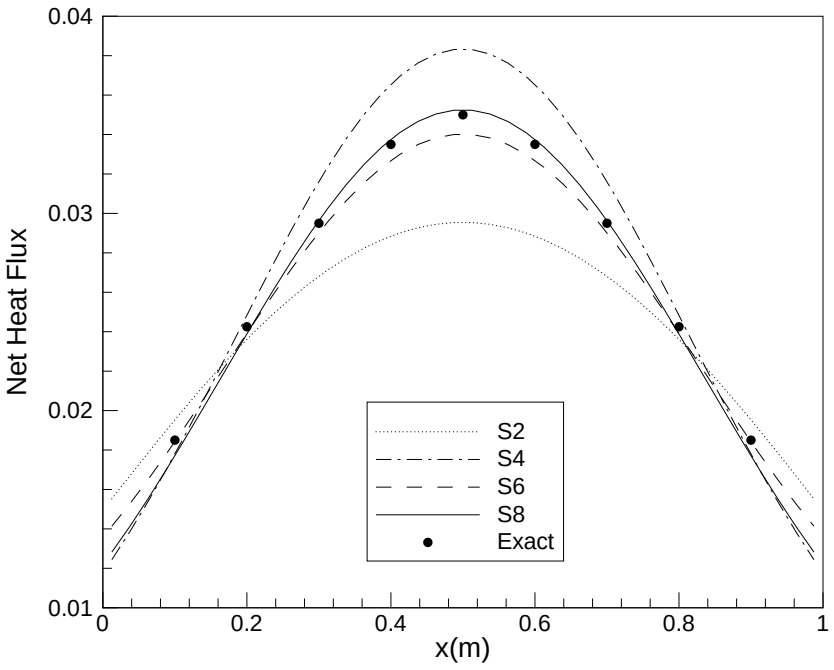

Figure 2: Net radiative heat fluxes ($\bar{q}_n$) on the $z = L_z$ wall of the cubical furnace at $y = 0.5m$.

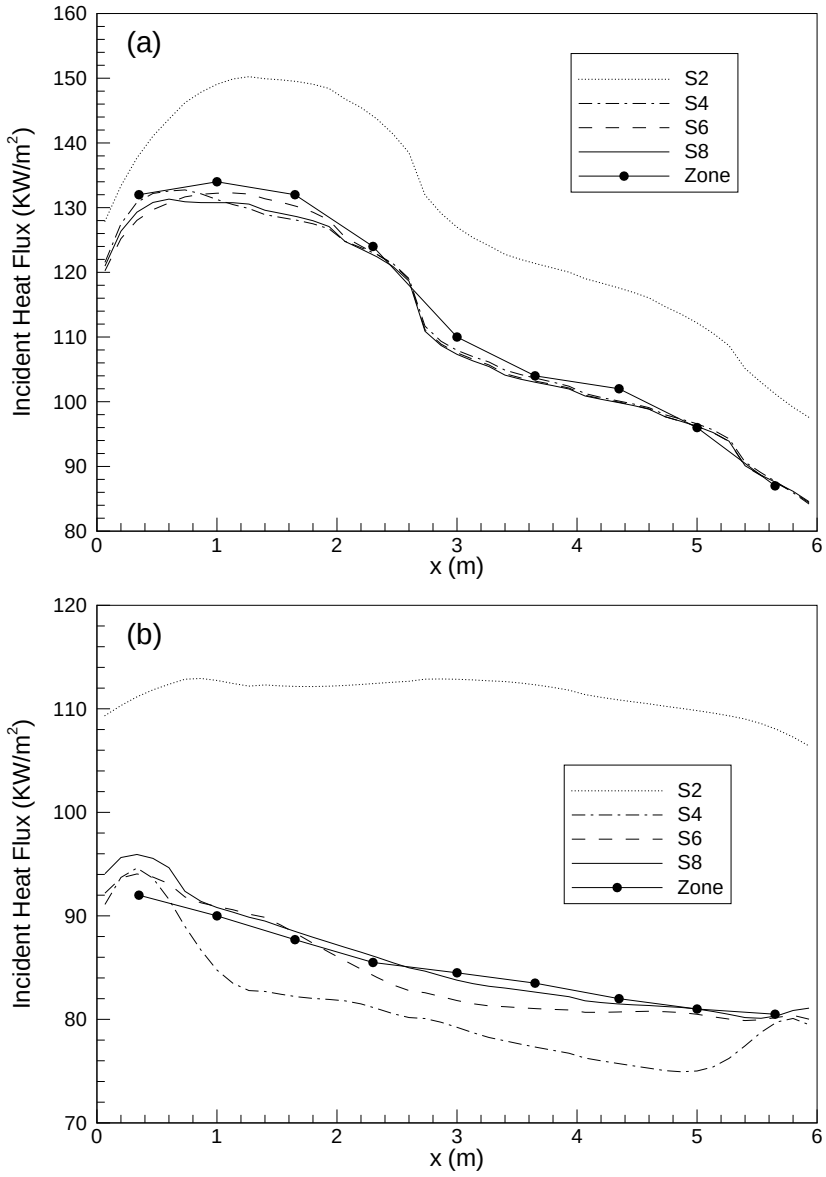

Figure 3: Incident radiative heat fluxes (q_{in}) on (a) $z = 0m$ (b) $z = 2m$ walls of the IFRF furnace at $y = 1m$.

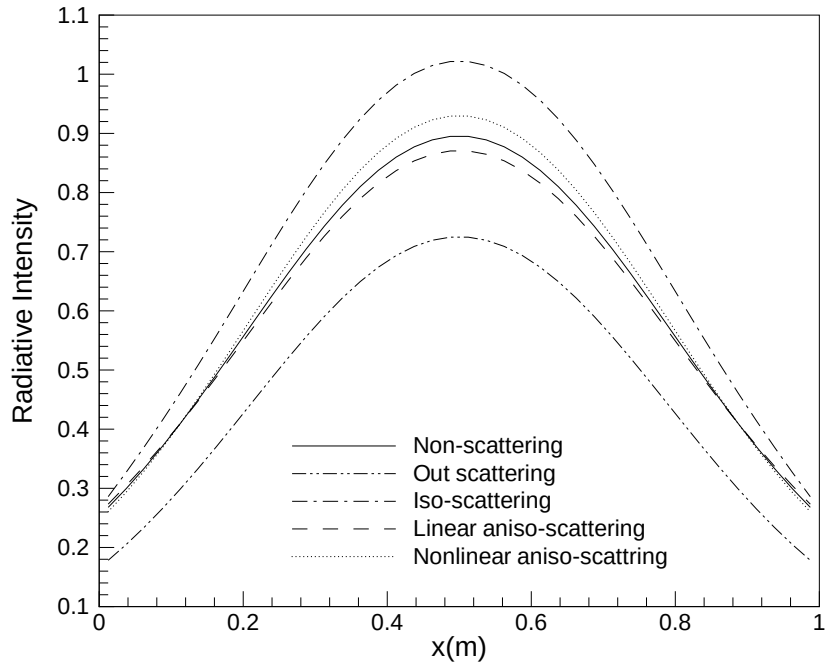

Figure 4: Results of the scattering effects in the cubical furnace. S_8 predictions of the radiative intensities ($\bar{I}$) at $y = 0.5m$ and $z = 0.5m$.

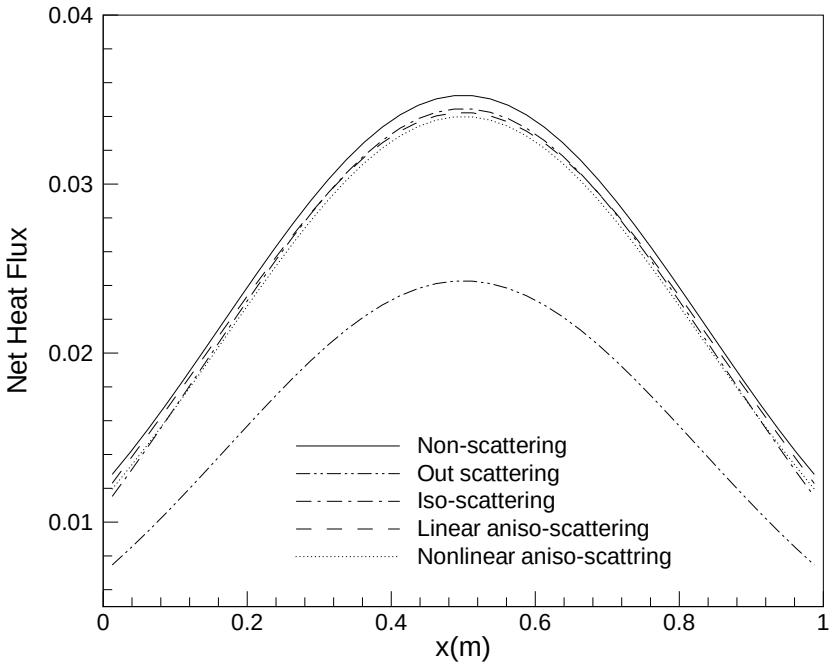

Figure 5: Results of the scattering effects in the cubical furnace. S_8 predictions of the net radiative heat fluxes ($\bar{q}_n$) at $y = 0.5m$ on the $z = L_z$ wall.

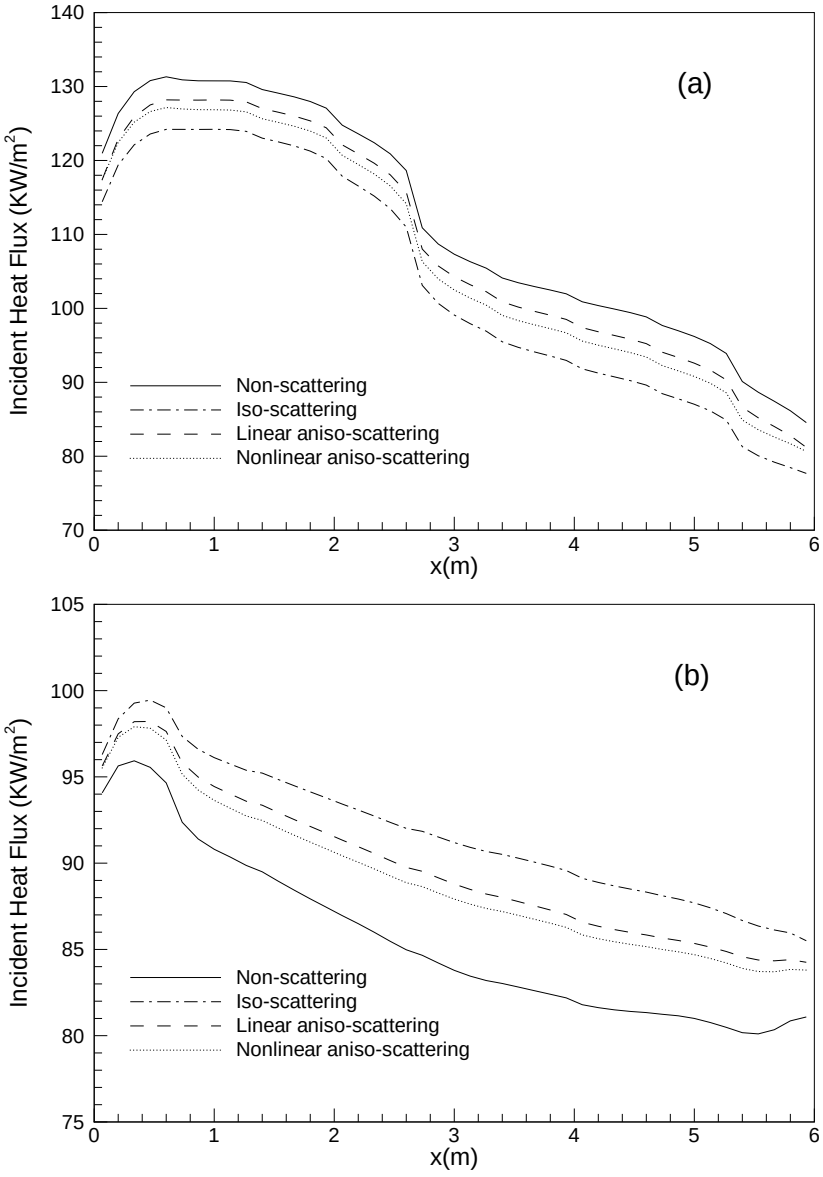

Figure 6: Results of the scattering effects in the IFRF furnace. S_8 results of the incident radiative heat fluxes (q_{in}) at $y = 1m$ on (a) $z = 0$ and (b) $z = 2m$ walls.